https://doi.org/10.5194/egusphere-2023-2958
Preprint. Discussion started: 23 January 2024

Accounting for Aerosols Effect in GHGSat Methane Retrieval

Qiurun Yu[1], Dylan Jervis[2], Yi Huang[1]

[1]Department of Atmospheric and Oceanic Sciences, McGill University, Montréal, QC, H3A 0B9, Canada
[2]GHGSat, Inc., Montréal, QC, H2W 1Y5, Canada

Correspondence to: Qiurun Yu (qiurun.yu@mail.mcgill.ca)

Abstract. GHGSat comprises a constellation of high spatial and spectral resolution satellites, specializing in monitoring methane emissions at 1.65 μm. This study investigates the ability to accurately retrieve both the methane mixing ratio enhancement (ΔX_{CH_4}) and aerosol optical depth (X_{AOD}) simultaneously from simulated GHGSat observations that incorporate angle-dependent scattering information. Results indicate that the polarity of ΔX_{CH_4} when neglecting aerosols changes from negative to positive as surface albedo increases, which is consistent with previous studies. Biases in ΔX_{CH_4} are most pronounced when X_{AOD} is not simultaneously retrieved, ranging from -3.0% to 6.3% with a 0.1 AOD, a 60° solar zenith angle, and a 0.2 surface albedo for the nadir-only retrieval. Using multiple satellite viewing angles during the GHGSat observation sequence with a scattering angle ranging from 100° to 140°, the study shows that the mean bias and standard deviation of ΔX_{CH_4} are within 0.2 % and 2.7% relative to the background. The correlation between simultaneously retrieved ΔX_{CH_4} and X_{AOD} shifts from positive to negative as surface albedo increases and aerosol asymmetry factor decreases, signifying a transition of the dominating aerosol effect from aerosol-only scattering to aerosol-surface multiple scattering. The variety of scattering angle ranges has little impact on the performance of the multi-angle viewing method. This study improves the understanding of the aerosol impact on the GHGSat ΔX_{CH_4} retrieval and provides guidance for improving future GHGSat-like point-source imagers.

1 Introduction

Aerosols can modify photon path length via their scattering and absorption effects and have been identified as one of the major sources of errors when retrieving greenhouse gases from spectrally resolved backscattered solar radiation in the shortwave infrared (SWIR) (Aben et al., 2007; Butz et al., 2009; Connor et al., 2016; Chen et al., 2017; Huang et al., 2021). Accurately assessing greenhouse gas emissions in the presence of aerosols remains a challenge. This is because unaccounted aerosols can either enhance or reduce the absorption of light by gases, depending on factors such as aerosol concentration, aerosol height distribution, viewing geometry, and surface albedo, among others (Butz et al., 2009; Frankenberg et al., 2012; Sanghavi et al., 2020). Houweling et al., (2005) analyzed Scanning Imaging Absorption Spectrometer for Atmospheric Chartography (SCIAMACHY) measurements of total column CO_2 over the Sahara and found that the unrealistically large CO_2 variability of 10% (37 ppm) of the total column was caused by mineral dust aerosols. Butz et al. (2009) found that if aerosols were not

https://doi.org/10.5194/egusphere-2023-2958
Preprint. Discussion started: 23 January 2024

considered, atmospheric CO_2 retrieval errors larger than 1% may occur when using the SCIAMACHY and Greenhouse gases Observing SATellite (GOSAT)-like observers. These errors are dependent on both surface albedo and the type of aerosols present. Huang et al. (2020) simulated Airborne Visible/Infrared Imaging Spectrometer – Next Generation (AVIRIS-NG) measurements for methane emissions. Their results show an underestimation of CH_4 resulting from aerosols, particularly those with high single scattering albedo and low asymmetry factor (such as water-soluble aerosols). These studies, among many others, underlined the importance of understanding the effect of aerosols on the remote sensing of greenhouse gases.

To account for the atmospheric scattering in SWIR satellite retrieval of greenhouse gas, a 'full-physics' retrieval requires simultaneously solving for the vertical profile of gas concentration, aerosol extinction, and the surface reflectivity by inversion of the radiance spectrum using a radiative transfer model (Butz et al., 2012; Jacob et al., 2022). However, this method is time-consuming and is likely to fail if the atmosphere is heavily polluted or if the surface is too dark (Lorente et al., 2021). In contrast to 'physics-based' methods, some proxy methods, which are much faster than full-physics retrievals and achieve similar precision and accuracy, have been proposed. To simultaneously retrieve the CO_2 total column and aerosol properties, the '3-band' retrieval exploits measurements of the absorption bands of O_2 (0.77 μm) and CO_2 (1.61 μm and 2.06 μm) to retrieve aerosol amount, height distribution, and size distribution based on a simple aerosol microphysical model (Butz et al., 2009). However, this approach requires additional consideration of the uncertainty of a prior estimate of CO_2 (Butz et al., 2012). According to Parker et al. (2020), methane mixing ratio ($\boldsymbol{X_{CH_4}}$) can be retrieved by using both CH_4 (1.65 μm) and the adjacent CO_2 band (1.61 μm) by taking advantage of the $\boldsymbol{X_{CH_4}/X_{co_2}}$ ratio without accounting for atmospheric scattering. However, this 'CO_2 proxy' method is subject to bias for sources that co-emit CH_4 and CO_2 such as gas flaring. Depending on the instrument design and its limitations, the approach to accounting for the effect of aerosols on greenhouse gas retrievals varies.

GHGSat, Inc. has developed a nano-satellite system that measures greenhouse gas emissions from individual industrial facilities (Varon et al., 2019). Its satellite achieves a combination of fine spatial resolution and spectral resolution by pointing at targeted methane point sources (Jervis et al., 2021; Jacob et al., 2022). As of the time of writing, GHGSat has launched a constellation of 11 commercial satellites (GHGSat-C1 to C11), which monitors methane emissions from natural gas industry operations, landfills, hydroelectric reservoirs, and oil sands operations among others (Calvello et al., 2017; Varon et al., 2019; Jacob et al., 2022; Maasakkers et al., 2022). However, industrial activities such as oil extraction and pre-treatment involve not only gaseous emission but also aerosol production (e.g., water-soluble and black carbon aerosols). The continued development of the GHGSat satellite requires identifying and minimizing the uncertainty in methane retrieval due to aerosol interference. Their newer satellites only target the CH_4 band; consequently, the above-mentioned 'proxy' methods to account for the aerosol effects do not apply to their instrument. An accurate GHGSat aerosol retrieval model for GHGSat would not only reduce the

https://doi.org/10.5194/egusphere-2023-2958
Preprint. Discussion started: 23 January 2024

uncertainty in their methane retrievals but also provide a new, aerosol data product, potentially making a high spatial resolution air quality measurement from the space.

The angular dependence of aerosol scattering allows space-borne observations of aerosol properties based on multi-angle measurements, providing the potential to mitigate aerosol-induced errors in current greenhouse gas satellite observations. Frankenberg et al. (2012) demonstrated that adding multiple satellite viewing angles to the Orbiting Carbon Observatory 2 (OCO-2)-like observations enhances the ability to retrieve aerosol properties. The aerosol information can in turn significantly decrease errors in the measurement of CO_2 and CH_4 total columns. However, this multi-angle viewing method was applied to area flux mappers which are designed to observe emissions on regional scales. There has been little study demonstrating how to retrieve aerosols using point source imagers like GHGSat. A method to co-retrieve aerosols and methane using GHGSat spectral content could address a gap in current research on point source imagers, improve the accuracy of their greenhouse gas retrieval, and provide greater details about aerosol and methane concentrations locally.

This study has three objectives. First, we assess how aerosols impact the accuracy of GHGSat methane mixing ratio enhancement ($\Delta \boldsymbol{X}_{\boldsymbol{CH_4}}$) retrievals when the aerosols are present but not retrieved. This assessment involves simulating GHGSat satellite observations for a wide range of simulated aerosol optical properties and surface albedo values to evaluate the distribution and magnitude of any resulting bias in $\Delta \boldsymbol{X}_{\boldsymbol{CH_4}}$ under different aerosol and surface conditions. Second, we simultaneously retrieve aerosol optical depth ($\boldsymbol{X}_{\boldsymbol{AOD}}$) and $\Delta \boldsymbol{X}_{\boldsymbol{CH_4}}$ using multi-angle viewing method in comparison with the $\Delta \boldsymbol{X}_{\boldsymbol{CH_4}}$-only retrieval under the same conditions. Finally, we study how the simulated retrieval errors vary with different scattering angles to examine the impact of observation angles on the performance of the simultaneous retrieval.

This paper is organized into four sections. Section 2 provides an overview of the atmospheric models, GHGSat instrument model, and the simultaneous retrieval methods for aerosols and methane. Section 3 evaluates the errors in GHGSat methane retrievals under various aerosol, surface, and satellite zenith angle conditions. Synthetic data is used to conduct retrievals under two scenarios: methane-only retrieval and the simultaneous retrieval of methane and aerosols using the multi-angle viewing method. A summary is presented in Section 4.

2 Method

2.1 Atmospheric Model

The Top of the Atmosphere (TOA) radiance detected by the satellite comes from both the direct and diffuse reflections. The incoming sunlight is reflected to space by the Earth's surface and atmospheric scatterers such as aerosols. When the solar beam travels through the atmosphere, it can partly be absorbed along its path by atmospheric absorbers, such as methane molecules

https://doi.org/10.5194/egusphere-2023-2958
Preprint. Discussion started: 23 January 2024

and aerosols. Additionally, multiple scattering processes occur between the surface and aerosol layers. To assess the radiative impact of aerosols in the GHGSat methane retrieval, a forward model is required to simulate GHGSat-measured solar radiation. The radiative transfer forward model of this study is DIScreet Ordinate Radiative Transfer (DISORT) version 4.0.99 (Stamnes et al., 1988). As one of the most general and versatile plane-parallel radiative transfer models, DISORT has been widely used for the remote sensing of greenhouse gases, aerosols, and clouds (Tzanis and Varotsos 2008; Wang et al. 2013; Boiyo et al. 2019). It can numerically compute satellite-measured radiance at different wavenumbers using discrete vertical coordinates. For each atmospheric layer, the spectral optical depth and single scattering albedo for atmospheric molecules are computed by using a rigorous line-by-line radiative transfer model (LBLRTM) over a 0.1 cm^2 interval (Clough et al., 2005). The mid-latitude summer profile is chosen as the default atmospheric state. The absorption of four main atmospheric absorptive gases (H_2O, CO_2, O_3, CH_4) at 45 layers is considered through line-by-line calculations.

To facilitate the analysis of aerosol-induced errors during the GHGSat CH_4 retrievals, this study focuses on the shortwave near-infrared band (1662 - 1672 nm). These bands cover the absorption lines which are mainly caused by CH_4. The surface is assumed to be Lambertian and we adopt the 16-stream approximation. With the specified viewing geometry and surface albedo, DISORT can calculate the solar radiation backscattered to space by the Earth's surface and atmosphere. For a clean atmosphere with a surface albedo of 0.2, the TOA upward radiance simulated by DISORT is shown in Fig. 1b. The solar zenith angle is 60°, and the satellite field of view is in the nadir position. In Fig. 1b, strong CH_4 absorptions are found around 1666 nm, affirming that the DISORT-simulated radiance is adequate for simulating the methane effect. With the TOA incoming solar radiance known (Fig. 1a), the TOA reflectance (Ref_λ^{TOA}) can be calculated following:

$$Ref_\lambda^{TOA} = \frac{radiance_\lambda^{TOA\uparrow}}{radiance_\lambda^{TOA\downarrow}}, \quad (1)$$

where $radiance_\lambda^{TOA\downarrow}$ and $radiance_\lambda^{TOA\uparrow}$ are the TOA downward and upward radiance at the wavelength λ. The radiance is in unit $Wm^{-2}sr^{-1}m^{-1}$. For the GHGsat retrieval only considering gas absorbers, the relative depth of the absorption line directly corresponds to the retrieved methane enhancement compared to the background. Therefore, Ref_λ^{TOA} is directly linked to the retrieved CH_4 enhancement and is shown in Fig. 1c.

https://doi.org/10.5194/egusphere-2023-2958
Preprint. Discussion started: 23 January 2024

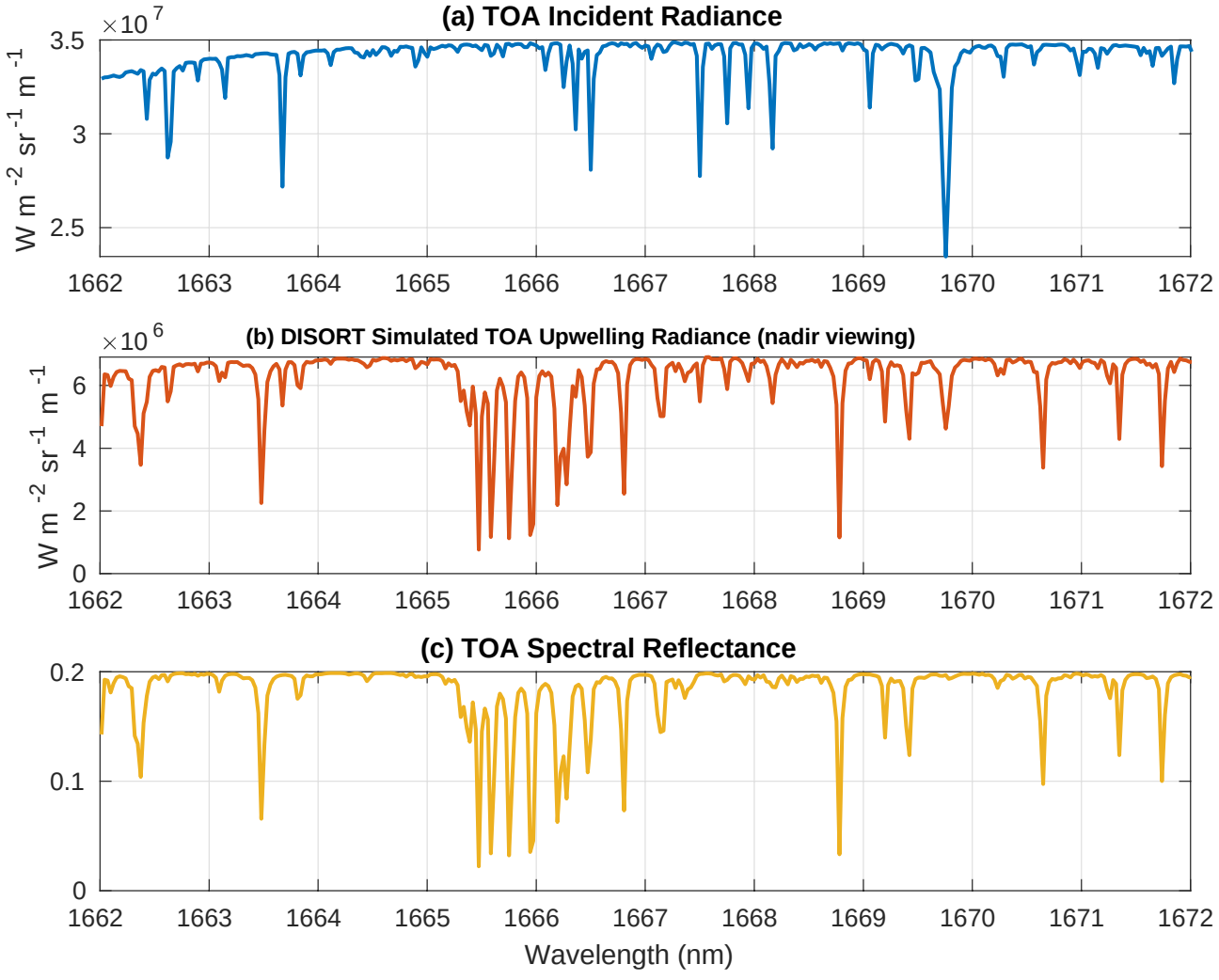

Figure 1. (a) TOA incoming solar radiance; (b) Simulated TOA upward radiance (nadir viewing); (c) Spectral reflectance (nadir viewing). Spectra are simulated with a surface albedo of 0.2 and a solar zenith angle of 60°.

2.2 Aerosol Settings

Many factors such as aerosol type, concentration, and height distribution can impact the radiance measurement. In this study, the aerosol types are predefined in the retrieval. We used climatological aerosol optical property values from Ayash et al. (2008) to account for the diverse range of particles found in industrial sites. For aerosols composed of multiple components, the single scattering albedo (SSA) spans from 0.86 to 0.98, while the asymmetry factor (g) ranges from 0.54 to 0.76. GHGsat mainly focuses on measuring CH_4 enhancement over methane hotspots, where CH_4 and the co-emitted aerosols are concentrated near the surface. To emulate the aerosol emissions from the industrial plume, one arbitrary aerosol layer is added near the surface between 1000 to 900 hPa. Considering the instrument limitation of one spectral band, the simplified treatment of aerosols in the forward model allows for a more direct physical interpretation of the effect of aerosols on methane retrievals.

https://doi.org/10.5194/egusphere-2023-2958
Preprint. Discussion started: 23 January 2024

We focus mainly on the AOD retrieval because this variable is highly representative of the aerosol radiation effect (Frankenberg et al., 2012; Yu and Huang, 2023). In this study, the simulated truth of AOD is 0.1 at SWIR (~0.3 AOD at 550nm). This threshold is selected in the retrieval because it is used as filter values in other XCH_4 retrieval studies (Lorente et al., 2021).

2.3 The Multi-angle Viewing Method

The multi-angle aerosol retrieval method proposed by Frankenberg et al. (2012) uses the radiance difference at various viewing geometries to retrieve aerosol information and takes advantage of the fact that aerosols scatter more light forward than backward. In this study, satellite azimuth angles are chosen as 0° and 180° to represent the forward-viewing and backward-viewing observations, respectively. Table 1 summarizes the angles used in the multi-angle viewing simulations. The scattering angle Θ is calculated following (Thompson et al., 2022) :

$$\Theta = 180° - \arccos[\cos\theta_1\cos\theta_2 + \sin\theta_1\sin\theta_2\cos(\varphi_1 - \varphi_2)] \quad (2),$$

where θ_1 and θ_2 are solar and satellite zenith angles, φ_1 and φ_2 are solar and satellite zenith angles, respectively. Fig. 2 shows the schematics of the multi-angle viewing method and its corresponding angles. This study assumes the Henyey-Greenstein Phase Function for aerosols (Toublanc, 1996), which defines the phase function following:

$$P_{HG}(\cos\Theta) = \frac{1-g^2}{(1-2g\cos\Theta+g^2)^{3/2}} \quad (3),$$

where g is the aerosol asymmetry factor. The high g value implies most of the scattered light is directed forward in the same general direction as the incident light.

https://doi.org/10.5194/egusphere-2023-2958
Preprint. Discussion started: 23 January 2024

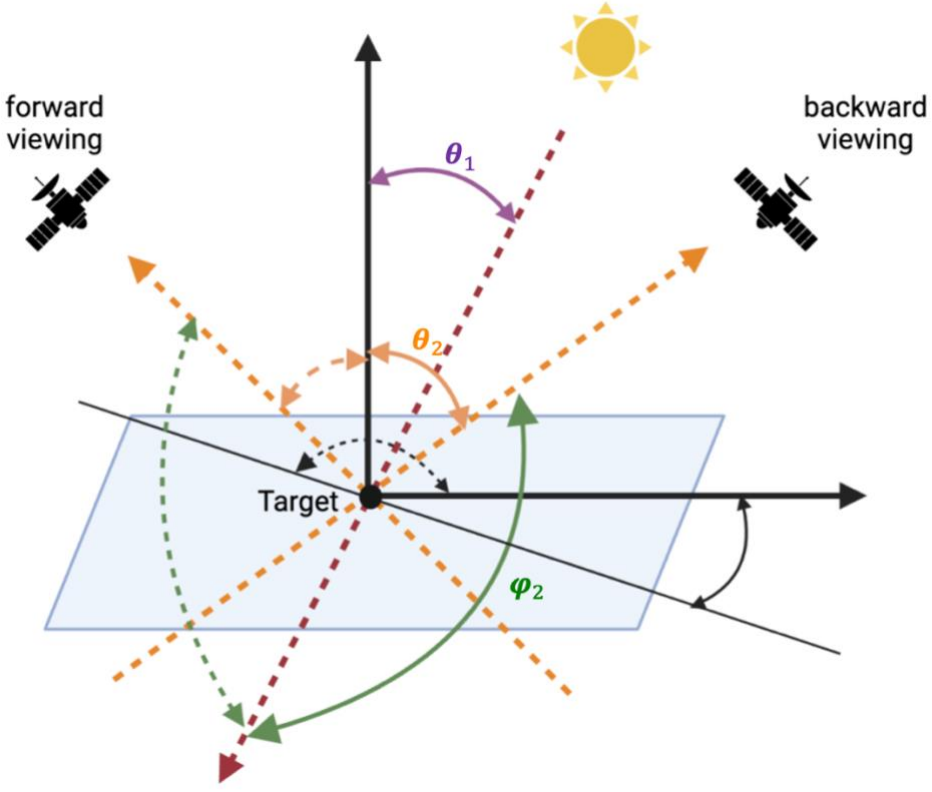

Figure 2. Schematic of a given solar and viewing geometry, as well as corresponding scattering angle for forward and backward viewing modes. Solar zenith θ_1, satellite zenith θ_2, and satellite azimuth angles φ_2 are indicated by the purple, orange, and green double arrow curves. For satellite viewing angles, the backward and forward viewing modes are represented by solid and dashed double arrow curves, respectively.

Table 1 Angles used in the multi-angle satellite viewing simulations for Sect. 3.1 and 3.2

	Solar zenith angle θ_1	Satellite zenith angle θ_2	Solar azimuth angle φ_1	Satellite azimuth angle φ_2	Scattering angle Θ
Forward viewing	60°	20°	180°	0°	100°
Nadir	60°	0°	180°	0°	120°
Backward viewing	60°	20°	180°	180°	140°

https://doi.org/10.5194/egusphere-2023-2958
Preprint. Discussion started: 23 January 2024

2.4 GHGSat Instrument Model

A nominal GHGSat measurement covers a targeted 12×15 km^2 area with approximately 25×25 m^2 pixel resolution and 0.3 nm spectral resolution (Jervis et al., 2021; Jacob et al., 2022). To simulate GHGSat measurements, this study focuses on the spectral region between 1662 nm and 1672 nm and applies a Gaussian broadening kernel of 0.3 nm full width at half maximum (FWHM). Using the multi-angle viewing method, the satellite observes the target position from different angles, transitioning from a forward view to a view looking directly downward (nadir), and finally to a backward view. During the observation sequences, the GHGSat spectrometer typically takes 200 images of closely overlapping atmospheric absorption spectrum. As an example, Fig. 3 displays the simulated GHGSat radiance corresponding to the solar geometry detailed in Table 1, under the assumption of a single layer of sulfate aerosols near the surface with an SSA of 1 and a g of 0.78. These simulations are based on a surface albedo of 0.2 and an AOD of 0.1 for illustration purposes. In the following discussions, a positive satellite zenith angle corresponds to an azimuth angle of 0° (forward viewing), while a negative zenith angle corresponds to an azimuth angle of 180° (backward viewing).

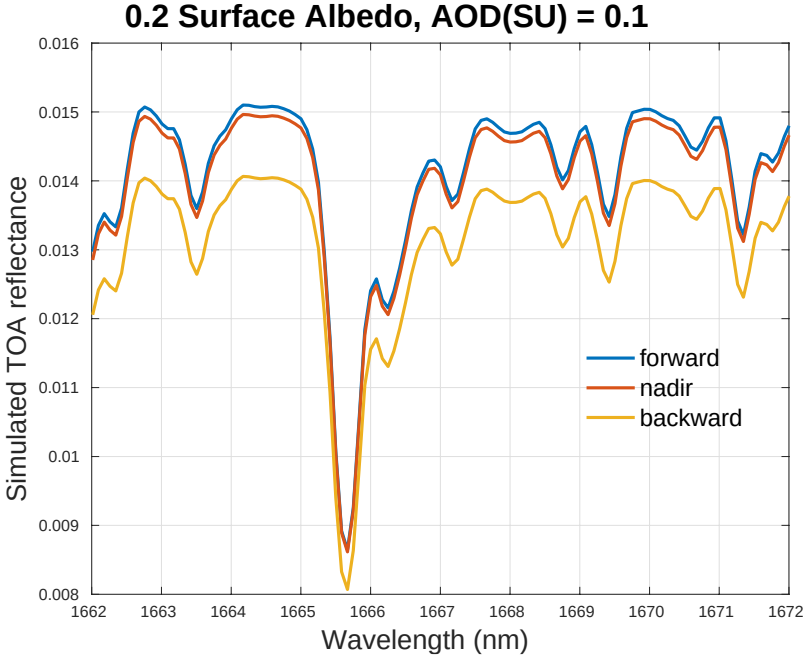

Figure 3. Simulated TOA reflectance observed by GHGSat instrument at a spectral resolution of 0.3 nm FWHM. The instrument observes the surface with an albedo of 0.2 from different viewing positions: forward viewing, nadir, and backward viewing following Table 1.

2.5 Retrieval Methods

Fig. 4 illustrates the steps of the simulated retrieval process in this study. First, we combine the atmospheric molecule optical properties calculated from LBLRTM with the aerosol optical properties to run the atmospheric model (DISORT). Then DISORT is further modified according to the GHGSat instrument design and the multi-angle viewing requirements to build a

https://doi.org/10.5194/egusphere-2023-2958
Preprint. Discussion started: 23 January 2024

complete forward model $\boldsymbol{F}(\boldsymbol{X})$ to simulate the TOA reflectance (Eq.(1)). $\mathbf{X}$ is the state vector, which includes elements such as methane mixing ratio $\boldsymbol{X}_{CH_4}$, aerosol optical depth $\boldsymbol{X}_{AOD}$, and the surface albedo $\boldsymbol{X}_{alb}$. The goal of the retrieval is to estimate $\Delta\boldsymbol{X}_{CH_4}$ for the ΔX_{CH_4}-only retrievals and to estimate $\Delta\boldsymbol{X}_{CH_4}$ and $\boldsymbol{X}_{AOD}$ for the simultaneous retrievals from the measurement vector $\boldsymbol{y}$:

$$\boldsymbol{y} = \boldsymbol{F}(\boldsymbol{X}) + \boldsymbol{\epsilon}_{\boldsymbol{y}} \quad (4)$$

where $\boldsymbol{\epsilon}_{\boldsymbol{y}}$ is the measurement error.

Full GHGSat retrieval consists of two steps: a scene-wide retrieval to estimate the background average state vector $\widehat{\boldsymbol{X}}$ and a per-cell retrieval to estimate the local methane plume enhancement. In this study, we focus on the per-cell retrieval assuming known background $\widehat{\boldsymbol{X}}$. In Jervis et al. (2021), a linearized forward model (LFM) is proposed for the GHGSat spatially resolved ΔX_{CH_4}-only retrieval.

$$\boldsymbol{F}^{LFM}(\boldsymbol{X}) = (\boldsymbol{X}_{alb} + b_1 n + b_2 n^2)\left[\boldsymbol{F}(\widehat{\boldsymbol{X}}) + (\boldsymbol{X}_{CH_4} - \widehat{\boldsymbol{X}_{CH_4}})\widehat{\boldsymbol{K}_{\boldsymbol{X}_{CH_4}}}\right]$$

$$= (\boldsymbol{X}_{alb} + b_1 n + b_2 n^2)\left[\boldsymbol{F}(\widehat{\boldsymbol{X}}) + \Delta\boldsymbol{X}_{CH_4}\widehat{\boldsymbol{K}_{\boldsymbol{X}_{CH_4}}}\right] \quad (5)$$

$\widehat{\boldsymbol{X}}$ is the linearization point, at which the state vector in the observation scene is assumed to be in the background state. $\boldsymbol{K}_{\widehat{\boldsymbol{X}}}$, the Jacobian that corresponds to different state vector elements, is a matrix of partial derivatives that describes how the simulated TOA reflectance changes with respect to the elements of the state vector.

$$\boldsymbol{K} = \frac{\partial \boldsymbol{F}(\boldsymbol{X})}{\partial \boldsymbol{X}} \quad (6)$$

To account for the bidirectional distribution of surface albedo and the per-pixel signal changes resulting from satellite motion, the forward model includes a second-order polynomial that is a function of the image frame index n (Jervis et al., 2021). In this study, we employed the LFM model and estimated $\Delta\boldsymbol{X}_{CH_4}$ and $\boldsymbol{X}_{alb}$ by minimizing the difference between the simulated instrument-measured $\boldsymbol{y}$ and $\boldsymbol{F}^{LFM}(\boldsymbol{X})$.

For simultaneous ΔX_{CH_4} and X_{AOD} retrievals, we added AOD as an additional variable of interest in the LFM as depicted below.

$$\boldsymbol{F}^{LFM} = (\boldsymbol{X}_{alb} + b_1 n + b_2 n^2)\left[\boldsymbol{F}(\widehat{\boldsymbol{X}}) + \Delta\boldsymbol{X}_{CH_4}\widehat{\boldsymbol{K}_{\boldsymbol{X}_{CH_4}}} + \boldsymbol{X}_{AOD}\widehat{\boldsymbol{K}_{\boldsymbol{X}_{AOD}}}\right] \quad (7)$$

The applicability of the simultaneous $\Delta\boldsymbol{X}_{CH_4}$ and $\boldsymbol{X}_{AOD}$ retrieval method mainly comes from two aspects: enhancing the methane gas retrieval accuracy by accounting for aerosols effect for GHGSat-like point source imagers and measuring aerosol plumes using such imagers.

https://doi.org/10.5194/egusphere-2023-2958
Preprint. Discussion started: 23 January 2024

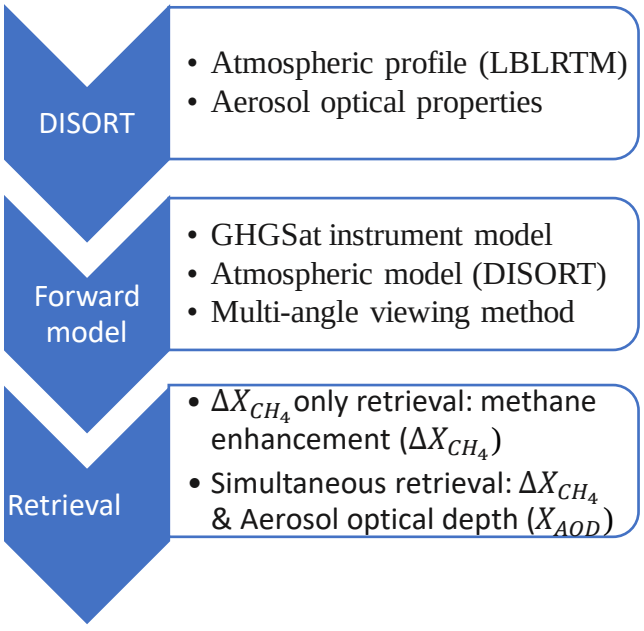

Figure 4. Schematic diagram of retrieval steps.

3. Simulated Retrieval Results

This paper aims to estimate the impact of aerosols on GHGSat methane retrieval, assess the validity of the multi-angle viewing method for the GHGSat aerosol and methane co-retrieval, and understand the algorithm's sensitivity to different input parameters, including surface albedo, SSA, g and satellite geometry. To achieve this, retrieval experiments were conducted using synthetic data, and the retrieval errors were estimated.

Fig. 5 depicts Jacobians with respect to the methane mixing ratio and AOD with different SSA and g values when the surface albedo is 0.2 and the solar zenith angle is 60°. A negative $\boldsymbol{K_X}$ value indicates that the reflectance at the TOA decreases as the value of the state vector element **X** increases. As expected, $\boldsymbol{K}_{CH_4}$ is negative considering the absorption properties of methane. Similarly, $\boldsymbol{K}_{AOD}$ is also negative in the case of absorbing aerosols (SSA=0.1). For strongly scattering aerosols (SSA=0.95) with high g (0.7) over the dark surface (0.2), $\boldsymbol{K}_{AOD}$ is slightly positive at the forward viewing position and negative at the backward viewing position (Fig. 5b). When the satellite is at the backward viewing position, the aerosol-only scattering is less pronounced because less light scatters towards the space in that direction, resulting in a negative $\boldsymbol{K}_{AOD}$. In contrast, in the forward viewing position, more light is scattered by aerosols toward the space, and this effect prevails over the effect of atmospheric absorption enhancement due to aerosol-surface multiple scattering, resulting in a slightly positive $\boldsymbol{K}_{AOD}$. This is particularly noticeable when the asymmetry factor, g, is low (0.1). In this case, the dominant factor is the shortening of the light path caused by aerosol-only scattering, which leads to a positive $\boldsymbol{K}_{AOD}$ regardless of the viewing angle (Fig. 5c). For aerosol with low g (0.1) over mid-range albedo (0.5), the competition between the aerosol-only scattering and aerosol-surface

https://doi.org/10.5194/egusphere-2023-2958
Preprint. Discussion started: 23 January 2024

multiple scattering result in a near zero $\boldsymbol{K}_{AOD}$ (Fig. 5e).

Fig. 5 also compares the Jacobians between satellite forward (scattering angle 100°) and backward (scattering angle 140°) viewing positions. With high SSA and g values, differences in aerosols Jacobian between the two angles increase, providing more information to the simultaneous retrieval. For simulated GHGsat retrieval using the multi-angle viewing technique, the scattering angle increases from 100° to 140° from forward viewing to backward viewing as depicted in Fig. 6. Considering that the simulated retrieval assumes the Henyey-Greenstein Phase Function for aerosols, the intensity of scattering energy decreases as the scattering angle increases, reducing the TOA reflectance. The greater the variation in TOA reflectance at various angles, the richer the aerosol information it can provide for simultaneous retrieval.

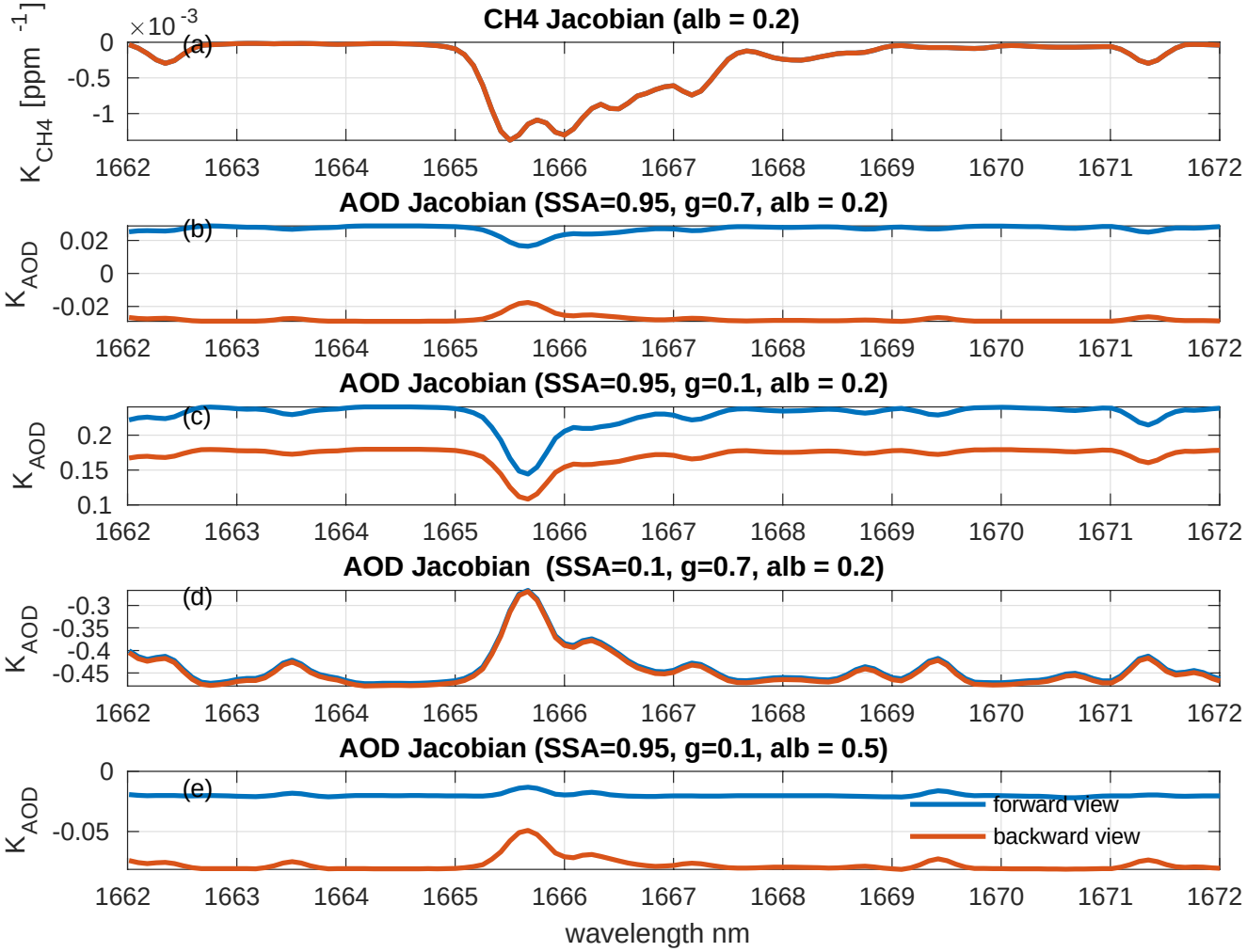

Figure 5. Jacobian of TOA reflectance with respect to (a) methane mixing ratio; (b) AOD with an SSA of 0.95, a g of 0.7, and a surface albedo of 0.2; (c) AOD with an SSA of 0.95, a g of 0.1, and a surface albedo of 0.2; (d) AOD with an SSA of 0.1, a g of 0.7, and a surface albedo of 0.2; (e) AOD with a SSA of 0.95, a g of 0.1, and a surface albedo of 0.5. Aerosols are concentrated near the surface and the forward and backward viewing angle settings follow Table 1.

https://doi.org/10.5194/egusphere-2023-2958
Preprint. Discussion started: 23 January 2024

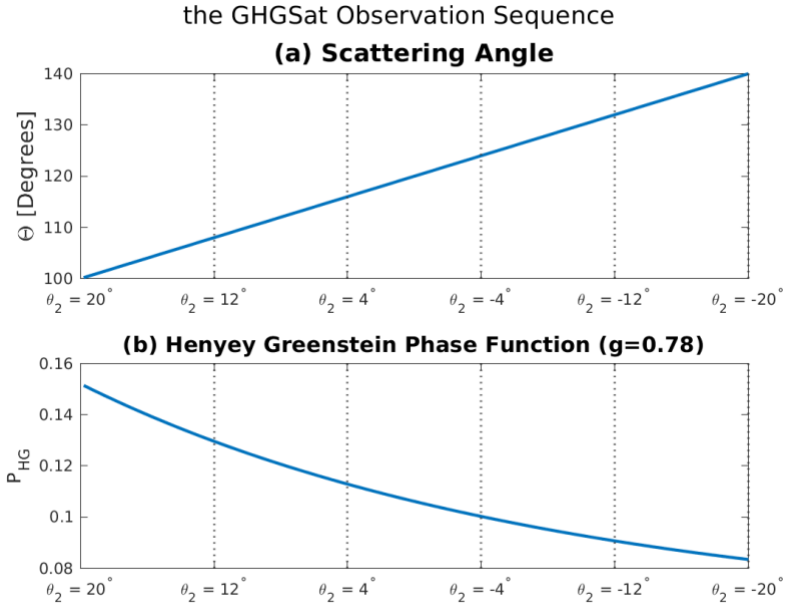

225 **Figure 6. (a) Scattering angles Θ and (b) Phase function P_{HG} for g =0.78 as a function of the satellite zenith angle θ_2 during GHGSat observation sequence when applying multi-angle viewing method with a maximum satellite zenith angle of 20°.**

As instrument measurements are always subject to noise and errors, it is important to include these in the simulated retrieval process to represent real-world conditions. During the simulated retrieval, white noise and 1/f errors with a magnitude of 0.2%
230 (calculated as the standard deviation of the individual noise fields) are added to the TOA reflectance. The background value for the methane mixing ratio is 1.7 ppm. The simulated truth of methane enhancement (ΔX_{CH_4}) and aerosol optical depth (X_{AOD}) are 0.1 ppm and 0.1, respectively. We performed 1000 independent retrievals for each aerosol and surface albedo setting and we quantified the mean bias and standard deviation of retrieved ΔX_{CH_4} relative to the background to represent the level of accuracy and consistency of retrieved data.

235 **3.1 The Impact of Incorporating AOD and Employing Multi-angle Viewing Methods**

To assess the extent to which incorporating aerosols and applying the multi-angle viewing method can improve the GHGsat methane retrieval, we conducted retrievals under four conditions: when aerosols are present but not retrieved for the (1) nadir-only methane retrieval and (2) the multi-angle viewing methane retrieval, and when aerosols and methane are co-retrieved (3) in the nadir viewing mode and (4) in the multi-angle viewing mode. Mean bias in the retrieved ΔX_{CH_4} and X_{AOD} are shown in
240 Fig.7. Fig. 7a and 7b indicate that the multi-angle viewing method alone has little impact on the methane retrieval accuracy for the methane-only retrieval. For extreme aerosol SSA and g values, the mean bias in ΔX_{CH_4} ranges from 6% to -25% when aerosols are neglected in the retrieval. After adding aerosols as an additional variable, the mean bias in ΔX_{CH_4} significantly

https://doi.org/10.5194/egusphere-2023-2958
Preprint. Discussion started: 23 January 2024

decreased to 0.32% (Fig. 7c). Applying the multi-angle viewing method with angles specific in Table 1 further diminishes the mean bias in ΔX_{CH_4} to 0.15% (Fig. 7d). This suggests that the good performance of aerosol and methane co-retrieval using multi-angle method largely comes from incorporating AOD as an additional retrieval variable.

As for the AOD retrieval performance, Fig. 7f suggests that applying the multi-angle viewing method yields better accuracy in the AOD retrieval than the nadir-only method, with the mean bias in X_{AOD} being 0.02. In theory, the multi-angle viewing method should provide more information than nadir viewing observations, especially for the aerosol retrieval. The relatively modest improvement observed with the multi-angle viewing method in our study compared to the substantial enhancement achieved by adding AOD alone may stem from the instrumental limitation of intensity-only measurements within a single spectral band. Nevertheless, our study continues to employ the multi-angle viewing method for the simultaneous aerosol and methane retrieval, as it yields the most significant improvement in retrieval accuracy and precision for both ΔX_{CH_4} and X_{AOD}.

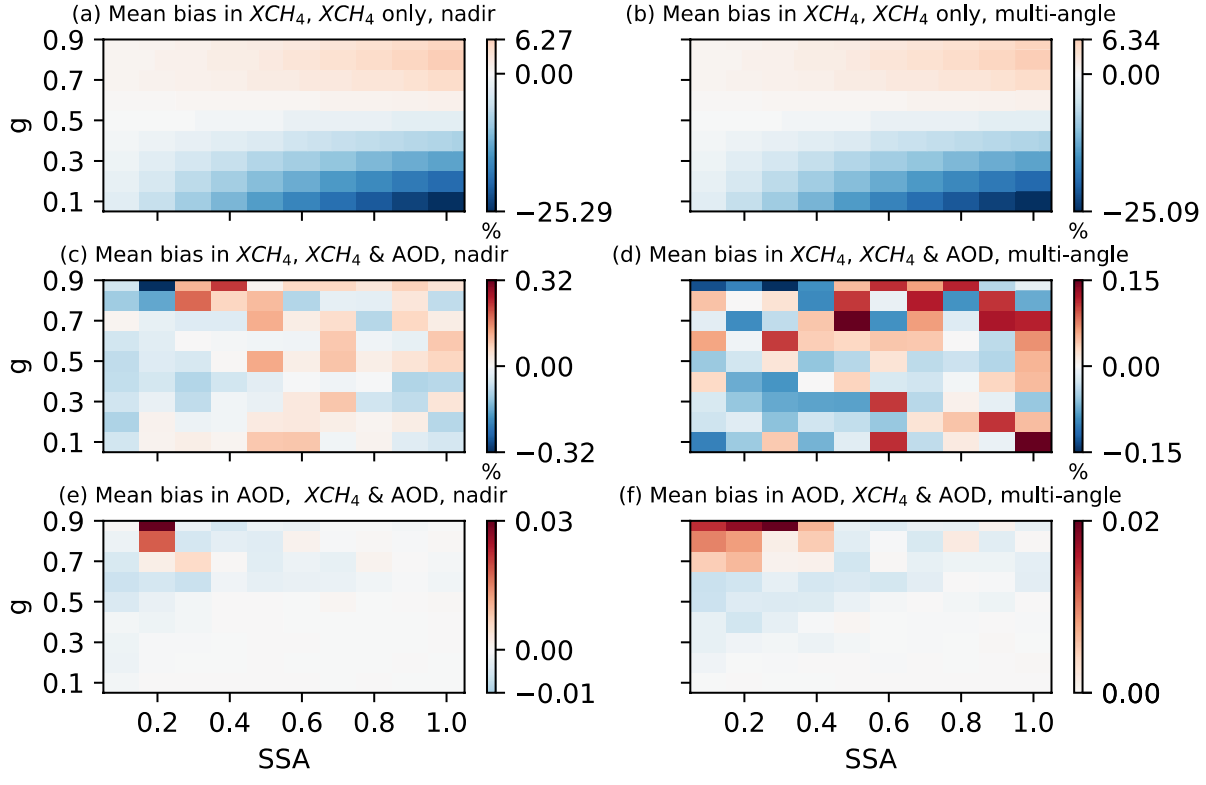

Figure 7. Left column: nadir-only viewing mode; Right column: multi-angle viewing mode (Table 1, scattering angle ranges from 100°-140°); Upper row: mean bias of retrieved ΔX_{CH_4} values when aerosols are present but not retrieved; Mid row: mean bias of retrieved ΔX_{CH_4} values when aerosols and methane are simultaneously retrieved; Lower row: mean bias of retrieved X_{AOD} values when aerosols and methane are simultaneously retrieved; Retrieval results are displayed as a function of aerosol SSA and g when surface albedo is 0.2. The simulated truth of ΔX_{CH_4} and X_{AOD} are 0.1 ppm and 0.1, respectively. The mean bias of ΔX_{CH_4} is calculated relative to the background methane mixing ratio.

https://doi.org/10.5194/egusphere-2023-2958
Preprint. Discussion started: 23 January 2024

3.2 Comparisons between the ΔX_{CH_4}-only Retrieval and Simultaneous ΔX_{CH_4} and X_{AOD} Retrieval

To examine the performance of different retrieval methods on different surfaces, we conducted simulated retrievals of ΔX_{CH_4} and X_{AOD} at a range of surface albedo and aerosol optical properties using the multi-angle viewing method. Fig. 8 illustrates the mean bias and standard deviations of retrieved ΔX_{CH_4} values under two scenarios: (1) when aerosols are present but not retrieved in the nadir-viewing mode and (2) when both ΔX_{CH_4} and X_{AOD} are retrieved simultaneously in the multi-angle viewing mode. The angle setting follows Table 1 and the surface albedo is fixed at 0.2.

When retrieving ΔX_{CH_4} without accounting for aerosols (Fig. 8a), results underestimate ΔX_{CH_4} for situations with low aerosol g and overestimate it in cases with high aerosol g. This occurs because when g is low, aerosols scatter more light back to space, reducing the absorption of CH_4. Conversely, when aerosol g is high, increased aerosol-surface multiple scatterings lead to greater atmospheric CH_4 absorption. For a 0.2 surface albedo, the maximum bias in ΔX_{CH_4} for ΔX_{CH_4}-only retrieval can reach -25% with extremely high SSA and low g values. These results are in agreement with other studies (Huang et al., 2020). Both increasing SSA and decreasing g enhance the radiation scatter back to Space, thereby decreasing the atmospheric methane absorptions. For typical optical property ranges of aerosols (SSA ∈ [0.86,0.98] and g ∈ [0.54,0.76]), mean bias in ΔX_{CH_4} falls between -3.0% to 6.3% for ΔX_{CH_4}-only nadir retrieval.

In contrast, Fig. 8b suggests that simultaneous ΔX_{CH_4} and X_{AOD} retrieval can significantly improve the accuracy of ΔX_{CH_4} retrieval. Using simultaneous retrieval can reduce the mean bias in ΔX_{CH_4} to within 0.1% (Table 2) for typical optical property ranges of aerosols. As for the consistency of the simultaneous retrieval, Fig. 8e indicates that the STD in ΔX_{CH_4} is slightly higher (~2.5%) than that in the ΔX_{CH_4}-only retrieval (~1.65%) when g and SSA are both high. This results from the near-zero AOD Jacobian values (Fig. 5b). Although aerosols have little effect on the TOA reflectance under these conditions, their inclusion in the simultaneous retrieval inevitably increases uncertainty in retrieved ΔX_{CH_4}. As for the accuracy and precision of the retrieved X_{AOD}, the mean bias in X_{AOD} is within 0.02 and the precision is within 0.1(Fig. 8c and 8f). For the AOD retrieval, the multi-angle method performs better when aerosols have high SSA and high g, which can be explained by the more pronounced AOD Jacobian differences between forward and backward viewing angles as indicated by Fig. 5b.

Table 2 Mean bias and STD in ΔX_{CH_4} and X_{AOD} for the ΔX_{CH_4}-only retrieval in the nadir viewing mode and simultaneous ΔX_{CH_4} and X_{AOD} retrievals in the multi-angle viewing mode with a 20° maximum satellite zenith angle. The simulated truth of AOD is 0.1. Mean bias and STD values in ΔX_{CH_4} are relative to the background CH_4 level.

SSA ∈ [0.86, 0.98], g ∈ [0.54, 0.76], sfc alb = 0.2					
	Mean bias in ΔX_{CH_4}	STD in ΔX_{CH_4}	Mean bias in X_{AOD}	STD in X_{AOD}	Corr coef btw ΔX_{CH_4} & X_{AOD}
ΔX_{CH_4}-only nadir retrieval	-3.0% ~ 6.3%	1.5% ~ 1.7%	-	-	-

https://doi.org/10.5194/egusphere-2023-2958
Preprint. Discussion started: 23 January 2024

ΔX_{CH_4}& X_{AOD} multi-angle retrievals	-0.1% ~ 0.1%	1.6% ~ 2.7%	0	0.02~0.05	-82% ~ 31%
Sfc alb ∈ [0.1, 0.5], SSA ∈ [0.86, 0.98], sfc alb = 0.2					
	Mean bias in ΔX_{CH_4}	STD in ΔX_{CH_4}	Mean bias in X_{AOD}	STD in X_{AOD}	Corr coef btw ΔX_{CH_4}& X_{AOD}
ΔX_{CH_4}-only nadir retrieval	-5.4% ~ 13.1%	1.6% ~ 1.7%	-	-	-
ΔX_{CH_4}& X_{AOD} multi-angle retrievals	-0.1% ~ 0.1%	1.8% ~ 2.6%	0	0.01~0.05	-81% ~ 52%
Sfc alb ∈ [0.1, 0.5], g ∈ [0.54, 0.76], sfc alb = 0.2,					
	Mean bias in ΔX_{CH_4}	STD in ΔX_{CH_4}	Mean bias in X_{AOD}	STD in X_{AOD}	Corr coef btw ΔX_{CH_4}& X_{AOD}
ΔX_{CH_4}-only nadir retrieval	-19.7% ~ 12.4%	1.5% ~ 1.7%	-	-	-
ΔX_{CH_4}& X_{AOD} multi-angle retrievals	-0.2% ~ 0.1%	1.5% ~ 2.7%	0	0.0~0.04	-79% ~ 42%
Sfc alb ∈ [0.1, 0.5], max(sat zenith) ∈ [0°,20°], SSA = 0.95, g = 0.7					
	Mean bias in ΔX_{CH_4}	STD in ΔX_{CH_4}	Mean bias in X_{AOD}	STD in X_{AOD}	Corr coef btw ΔX_{CH_4}& X_{AOD}
ΔX_{CH_4}-only multi-angle retrieval	-5.7%~12.5%	1.56%~1.64%	-	-	-
ΔX_{CH_4}& X_{AOD} multi-angle retrievals	-0.1%~0.11%	1.8%~2.2%	0	0.01~0.03	-66%~39%

https://doi.org/10.5194/egusphere-2023-2958
Preprint. Discussion started: 23 January 2024

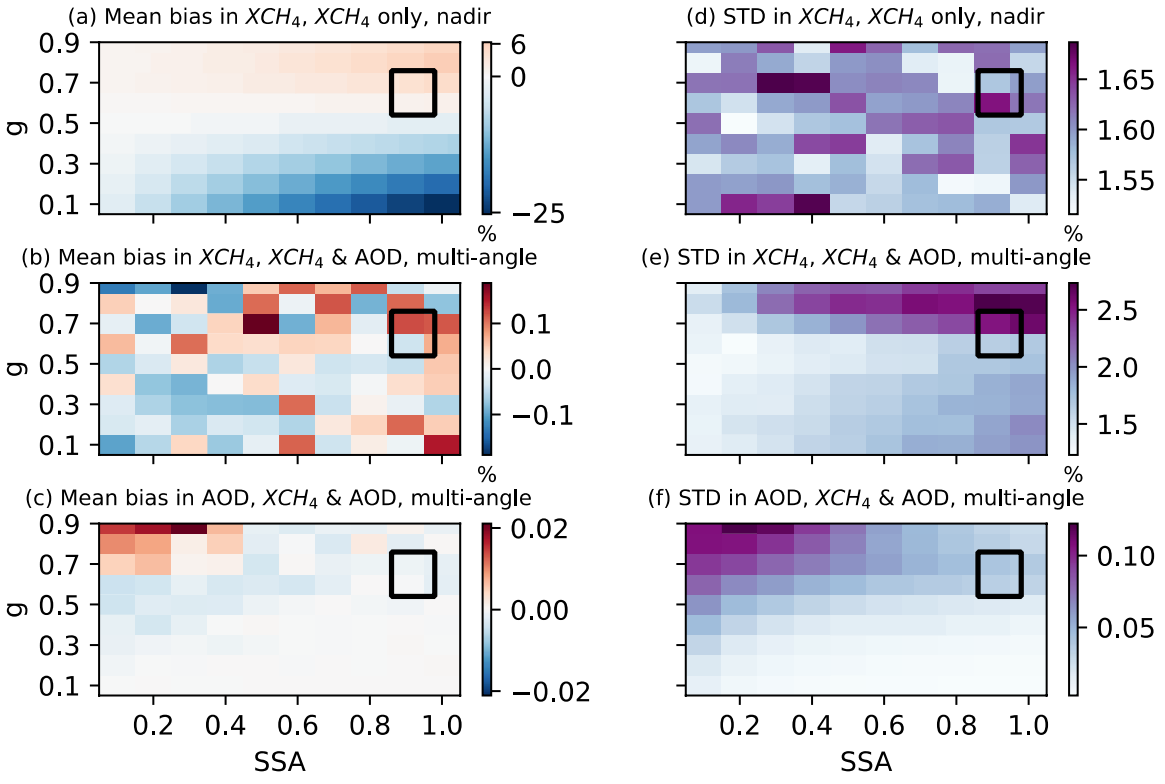

Figure 8. (a) Mean bias and (d) standard deviations (STD) of retrieved ΔX_{CH_4} values when aerosols are present but not retrieved in the nadir viewing mode; (b) Mean bias and (e) STD of retrieved ΔX_{CH_4} values for simultaneous ΔX_{CH_4} and X_{AOD} retrievals in the multi-angle viewing mode; (c) Mean bias and (f) STD of retrieved X_{AOD} values for simultaneous ΔX_{CH_4} and X_{AOD} retrievals in the multi-angle viewing mode; Retrieval results are displayed as a function of aerosol SSA and g when surface albedo is 0.2 and scattering angle ranges from 100°-140° (solar zenith angle 60° and maximum satellite zenith angle 20°). The simulated truth of ΔX_{CH_4} and X_{AOD} are 0.1 ppm and 0.1, respectively. The black box represents the typical values for aerosol optical property ranges (SSA ∈ [0.86, 0.98] and g ∈ [0.54, 0.76]) in the retrieval.

Since the underlying surface can largely determine the retrieval performance, we further explored the accuracy and precision of ΔX_{CH_4}-only retrieval and simultaneous retrieval under different surface albedo conditions. Fig. 9 illustrates the distribution of retrieval errors (mean bias and STD) for ΔX_{CH_4}-only retrieval and simultaneous retrievals when aerosol g is fixed as 0.7. As shown in Fig. 9a, neglecting aerosols results in an overestimation (underestimation) of the retrieved ΔX_{CH_4} with high (low) surface albedo. These results are in agreement with other studies (Butz et al., 2009; Huang et al., 2020) despite the differences in retrieval variables, experiment settings, and instruments. High surface albedo enhances the surface and aerosol multiple scattering, thereby increasing methane absorptions. When surface albedo is low, aerosol-only scattering predominates and reduces methane absorptions. Therefore, in the case of ΔX_{CH_4}-only retrieval, the bias is most pronounced (~25%) when both aerosol SSA and surface albedo are extremely high. Therefore, it is advisable to refrain from performing methane retrievals over highly reflective surfaces. For aerosol SSA (0.86-0.98) and surface albedo (0.1-0.5) values commonly encountered, the

https://doi.org/10.5194/egusphere-2023-2958
Preprint. Discussion started: 23 January 2024

mean bias in ΔX_{CH_4} for ΔX_{CH_4}-only retrieval ranges from -5.4% to 13.1% when g is fixed at 0.7.

When simultaneously retrieving methane and aerosols, Fig. 9b suggests the mean bias of ΔX_{CH_4} is significantly reduced to 0.1% by comparing with the ΔX_{CH_4}-only retrieval. The STD of the retrieved methane is slightly higher when high SSA aerosols are present over low albedo surfaces. This is explained by the near-zero AOD Jacobian values (Fig. 5b) as previously discussed. Moreover, the STD of the retrieved methane and AOD is a bit higher when SSA is extremely low (0.1). This decrease in retrieval precision results from the positive values in AOD Jacobian, as well as minimal differences in AOD Jacobian between forward and backward viewing (Fig. 5d) considering the strong absorbing characteristics of aerosols. In this scenario, it is challenging to distinguish between aerosols and surface, thereby affecting the CH_4 and aerosol retrieval. The mean bias and STD in retrieved X_{AOD} are within 0.01 and 0.1, respectively. In general, the multi-angle viewing technique demonstrates higher accuracy compared with the ΔX_{CH_4}-only retrieval, especially for aerosols with stronger scattering ability.

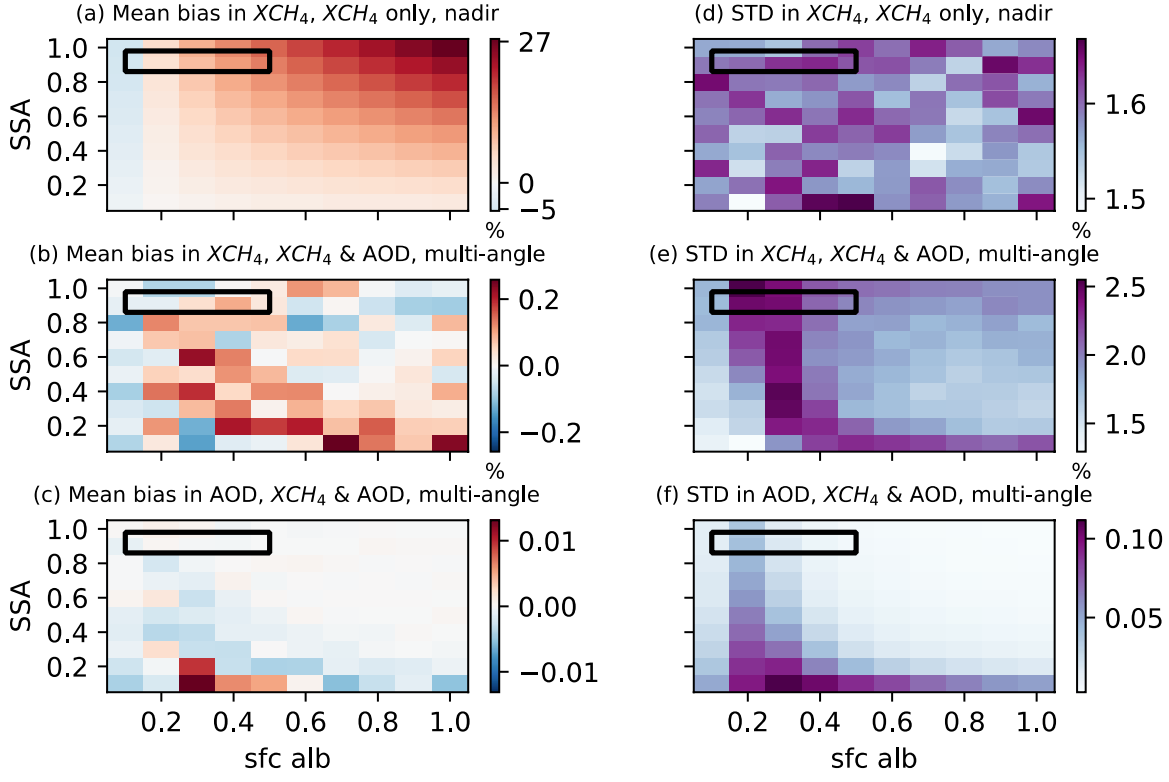

Figure 9. (a) Mean bias and (d) standard deviations (STD) of retrieved ΔX_{CH_4} values when aerosols are present but not retrieved in the nadir viewing mode; (b) Mean bias and (e) STD of retrieved ΔX_{CH_4} values for simultaneous ΔX_{CH_4} and X_{AOD} retrievals in the multi-angle viewing mode; (c) Mean bias and (f) STD of retrieved X_{AOD} values for simultaneous ΔX_{CH_4} and X_{AOD} retrievals in the multi-angle viewing mode; Retrieval results are displayed as a function of surface albedo and aerosol SSA when aerosol g is 0.7 and scattering angle ranges from 100°-140°. The simulated truth of ΔX_{CH_4} and X_{AOD} are 0.1 ppm and 0.1, respectively. The black box represents the typical values for aerosol optical property and surface albedo ranges (sfc alb ∈ [0.1, 0.5] and SSA ∈ [0.86, 0.98]) in the retrieval.

https://doi.org/10.5194/egusphere-2023-2958
Preprint. Discussion started: 23 January 2024

Apart from SSA, it is also interesting to examine how the retrieval bias varies under different combinations of aerosol asymmetry factor and surface albedo. Fig. 10 presents retrieval errors (mean bias and STD) for ΔX_{CH_4}-only retrieval and simultaneous retrievals when aerosol SSA is fixed as 0.95. For ΔX_{CH_4}-only retrieval, ΔX_{CH_4} is underestimated (overestimated) with low (high) surface albedo especially when g is small. These errors arise because aerosols with low g over dark surfaces tend to scatter more light towards the space. However, when the surface is bright, it reflects a larger proportion of light towards aerosols, and aerosols with low g tend to scatter this light back to the surface again, thereby enhancing methane absorption. The maximum bias in ΔX_{CH_4} for ΔX_{CH_4}-only retrieval is around -50% when both aerosol g and surface albedo are extremely low. For the typical values of g (0.54,0.76) and surface albedo (0.1-0.5), neglecting aerosols results in a mean bias in ΔX_{CH_4} ranging from -19.7% to 12.4%. However, through simultaneous retrieval, this bias can be reduced to -0.2% to 0.1% (Table 2). As for the STD of ΔX_{CH_4} in the simultaneous retrieval, an increase in surface albedo and a decrease in g intensify the competition between enhanced surface-aerosol multiple scattering and increased aerosol-only scattering toward the space. This competition can cause near-zero AOD Jacobian values, resulting in a slight reduction in the ΔX_{CH_4} retrieval precision (Fig. 5b and 5e). In the presence of strongly scattering aerosols (SSA=0.95), the mean bias and STD in X_{AOD} fall within 0.001 and 0.04, respectively, indicating the good performance of the simultaneous retrieval in AOD retrieval.

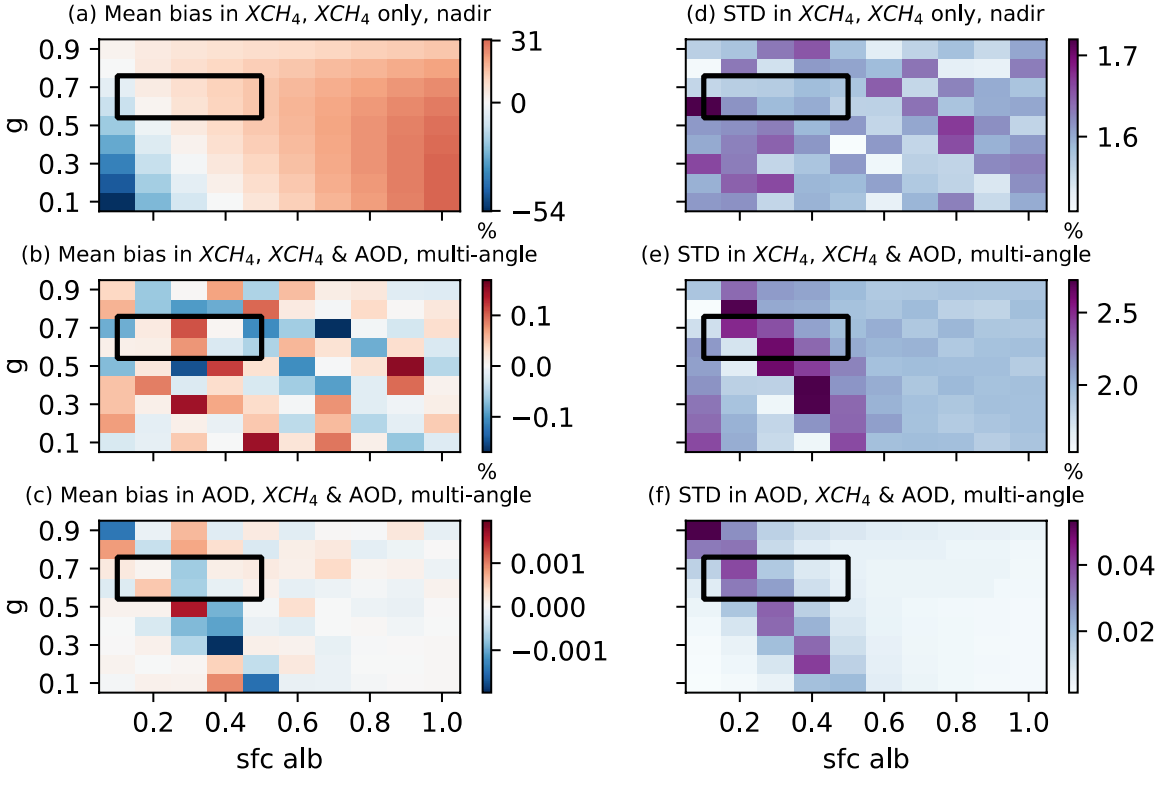

https://doi.org/10.5194/egusphere-2023-2958
Preprint. Discussion started: 23 January 2024

Figure 10. (a) Mean bias and (d) standard deviations (STD) of retrieved ΔX_{CH_4} values when aerosols are present but not retrieved; (b) Mean bias and (e) STD of retrieved ΔX_{CH_4} values for simultaneous ΔX_{CH_4} and X_{AOD} retrievals; (c) Mean bias and (f) STD of retrieved X_{AOD} values for simultaneous ΔX_{CH_4} and X_{AOD} retrievals; Retrieval results are displayed as a function of surface albedo and aerosol g when aerosol SSA is 0.95 and scattering angle ranges from 100°-140°. The simulated truth of ΔX_{CH_4} and X_{AOD} are 0.1 ppm and 0.1, respectively. The black box represents the typical values for aerosol optical property and surface albedo ranges (sfc alb ∈ [0.1, 0.5] and g ∈ [0.54, 0.76]).

Overall, for simultaneous ΔX_{CH_4} and X_{AOD} retrievals using the multi-angle viewing method, the retrieved ΔX_{CH_4} and X_{AOD} values generally match very well with the simulated truth. The mean bias and STD in ΔX_{CH_4} fall within the range of 0.2% and 2.5%, respectively. Similarly, the mean bias and STD in X_{AOD} are within 0.02 and 0.1, respectively, across various aerosol optical properties and surface albedo conditions. It should be noted that under certain conditions characterized by near zero AOD Jacobian values, such as scenarios with high SSA and high g values over low albedo surface, and high SSA and low g values over moderately reflective surface, or positive AOD Jacobian values when SSA is extremely low over surfaces with medium to high albedo, we observe a slightly higher STD in ΔX_{CH_4} and X_{AOD} retrievals.

3.3 The Effect of Satellite Zenith Angle on Simultaneous Retrieval

The discussions above have proved that using the multi-angle viewing method for simultaneous ΔX_{CH_4} and X_{AOD} retrievals can significantly improve the retrieval accuracy of ΔX_{CH_4} by comparing it with the ΔX_{CH_4}-only nadir retrieval. It is still worth investigating whether the retrieval results are highly dependent on the chosen satellite zenith angles. Table 3 lists a bunch of satellite zenith angles that are tested in both the ΔX_{CH_4}-only retrieval and the simultaneous retrieval. A larger magnitude of the satellite zenith angle means a broader range of the scattering angle and more distinct differences in TOA reflectance between different satellite viewing positions.

Considering aerosols with an AOD of 0.1, a SSA of 0.95, and a g of 0.7, the mean bias and STD for the ΔX_{CH_4}-only retrieval and simultaneous retrieval as a function of surface albedo and the maximum magnitude of the satellite zenith angle is shown in Fig. 11. If aerosols are neglected, the retrieved ΔX_{CH_4} are always overestimated except for the extremely low surface albedo (0.1) condition. The retrieval bias magnitude escalates with the growing maximum magnitude of the satellite zenith angle. A larger satellite zenith angle brings in a longer light path, which enhances atmospheric absorption and introduces larger retrieval errors. The maximum mean bias in ΔX_{CH_4} for ΔX_{CH_4}-only retrieval can exceed 80% when the satellite zenith angle exceeds 70°. For typical GHGSat satellite zenith angle (10°-20°) and surface albedo (0.1-0.5) ranges, the mean bias in ΔX_{CH_4} for ΔX_{CH_4}-only retrieval is -5.7%~12.5%. For simultaneous ΔX_{CH_4} and X_{AOD} retrieval, the mean bias remains below 0.2% and it varies little with the chosen satellite zenith angle. This suggests that the multi-angle viewing method is effective for GHGSat-like satellites, regardless of their observation swath. The better retrieval performance of simultaneous retrieval in the multi-angle viewing mode largely contributed from adding AOD as an additional predictor instead of applying the multi-angle method, considering GHGSat Satellite is an intensity-only instrument targeting one specific band.

https://doi.org/10.5194/egusphere-2023-2958
Preprint. Discussion started: 23 January 2024

For the STD in ΔX_{CH_4} from the simultaneous retrieval, its magnitude experiences a slight increase and then decreases as the satellite zenith angle magnitude increases. This happens because, with the increase of the satellite's zenith angle, more energy scatters back to space while a longer light path leads to greater atmospheric absorption. At a specific point, the aerosol Jacobian approaches zero, which introduces relatively high uncertainty into the simultaneous retrieval process.

Table 3 Satellite zenith angle ranges tested for ΔX_{CH_4}-only retrieval and simultaneous ΔX_{CH_4} and X_{AOD} retrievals using the multi-angle viewing method. The solar zenith angle is 60°.

Satellite zenith angle range	-10° ~ 10°	-20° ~ 20°	-30° ~ 30°	-40° ~ 40°	-50° ~ 50°	-60° ~ 60°	-70° ~ 70°	-80° ~ 80°
Scattering angle range	110 ° ~ 130°	100 ° ~ 140°	90° ~ 150°	80° ~ 160°	70° ~ 170°	60° ~ 180°	50° ~ 180°	40° ~ 180°

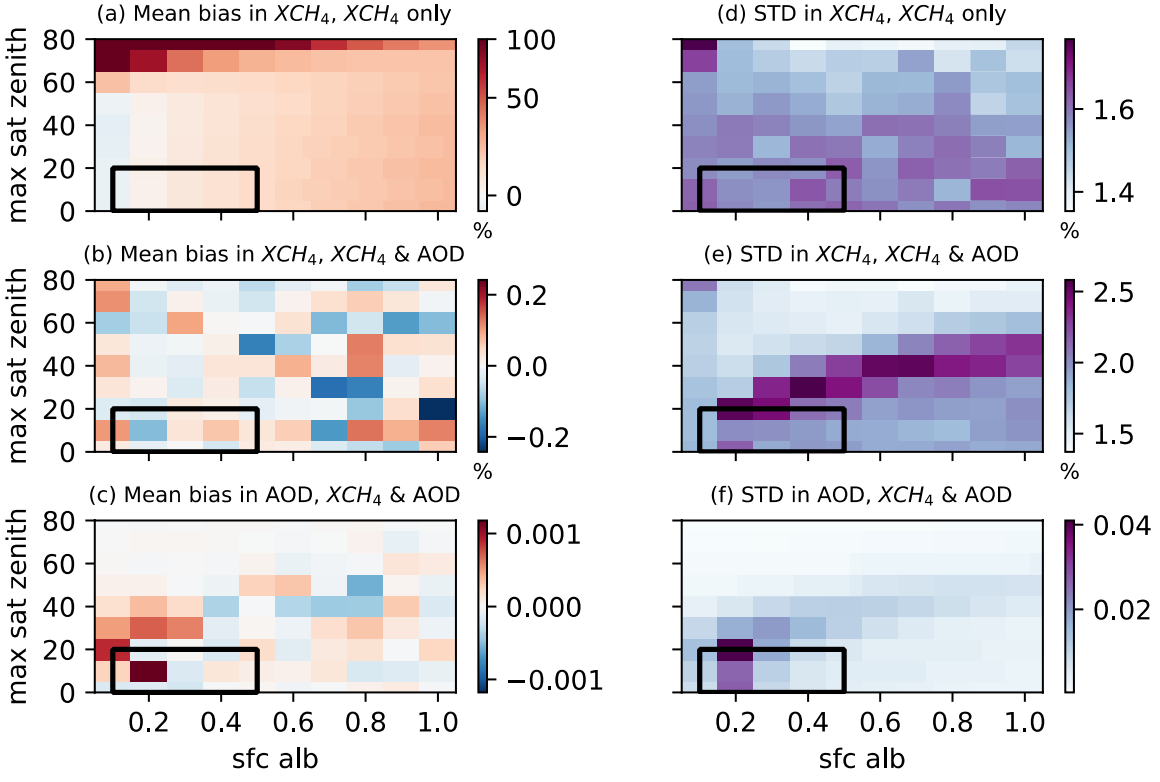

Figure 11. (a) Mean bias and (d) standard deviations (STD) of retrieved ΔX_{CH_4} values when aerosols are present but not retrieved; (b) Mean bias and (e) STD of retrieved ΔX_{CH_4} values for simultaneous ΔX_{CH_4} and X_{AOD} retrievals; (c) Mean bias and (f) STD of retrieved X_{AOD} values for simultaneous ΔX_{CH_4} and X_{AOD} retrievals; Retrieval results are displayed as a function of surface albedo and maximum magnitude of satellite zenith angle when aerosol SSA is 0.95

https://doi.org/10.5194/egusphere-2023-2958
Preprint. Discussion started: 23 January 2024

and g is 0.7, and the solar zenith angle is 60°. Satellite is in the multi-angle viewing mode. The black box represents the typical values for GHGSat satellite zenith angle and surface albedo ranges (max(sat zenith) $\theta_2 \in$ [0°, 20°] and sfc alb $\in$ [0.1, 0.5]).

3.4 Relationship between Retrieved ΔX_{CH_4} and ΔX_{AOD} from the Simultanous Retrieval

Fig. 12 illustrates the correlation coefficients between the retrieved ΔX_{CH_4} and X_{AOD} for various combinations of SSA, g, surface albedo, and satellite zenith values. The simultaneous retrieval is conducted under four specific conditions using the multi-angle viewing method: (1) when the surface albedo is 0.2, (2) when the g is 0.7, (3) when the SSA is 0.95, (4) when the SSA is 0.95 and g is 0.7. For conditions (1) to (3), the angle setting follows Table 1, while for condition (4), the angle settings are based on Table 3.

Fig. 12a suggests that ΔX_{CH_4} and X_{AOD} are negatively correlated for high g values and negatively correlated for low g values when the surface is dark. A high g results in more concentrated forward scattering towards the ground, causing more atmospheric absorption via aerosol-surface multiple scattering. To maintain the relative depth of the CH_4 absorption spectra, less ΔX_{CH_4} needs to be retrieved to balance the effect of increasing X_{AOD}. In Fig. 12b, ΔX_{CH_4} and X_{AOD} are positively correlated for low albedo surfaces and negatively correlated for mid and high albedo surfaces when g is 0.7. With a dark surface, the increase of aerosols scatters a greater amount of light back to space, leaving less light to interact with CH_4. Consequently, a larger ΔX_{CH_4} is retrieved to counterbalance the impact of increasing X_{AOD}. Fig. 12c shows that the correlation between ΔX_{CH_4} and X_{AOD} changes from positive to negative with the increase of g and surface albedo when SSA is 0.95. This pattern occurs because of the shift in dominant aerosol-involved physical processes from the aerosol-only scattering effect to the aerosol and surface multiple scattering effects. Fig. 12d shows that for aerosols with an SSA of 0.95 and a g of 0.7, ΔX_{CH_4} and X_{AOD} are positively (negatively) correlated at low(high) albedo. With the increase of the satellite zenith angle, the magnitude of the correlation coefficient first increases and then decreases, suggesting that it is still beneficial to apply large scattering angle ranges in the multi-angle viewing method to better distinguish aerosols and methane.

When considering a surface with an albedo of 0.2, a SSA from 0.86 to 0.98, and a g from 0.54 to 0.76, the correlation coefficient between the retrieved ΔX_{CH_4} and X_{AOD} falls within the range of -82% to 31%. Similarly, when the SSA is maintained between 0.86 and 0.98, the surface albedo varies from 0.1 to 0.5, and g is fixed at 0.7, the correlation coefficient ranges from -79% to 42%. Lastly, for cases where g ranges from 0.54 to 0.76, the surface albedo spans from 0.1 to 0.5, and SSA is set at 0.95, the correlation coefficient varies from -81% to 52%. In general, The pattern in Fig.12 is similar to the ΔX_{CH_4} STD pattern in Fig. 8-11, which confirms that the highly correlated ΔX_{CH_4} and X_{AOD} results in larger STD in ΔX_{CH_4}.

https://doi.org/10.5194/egusphere-2023-2958
Preprint. Discussion started: 23 January 2024

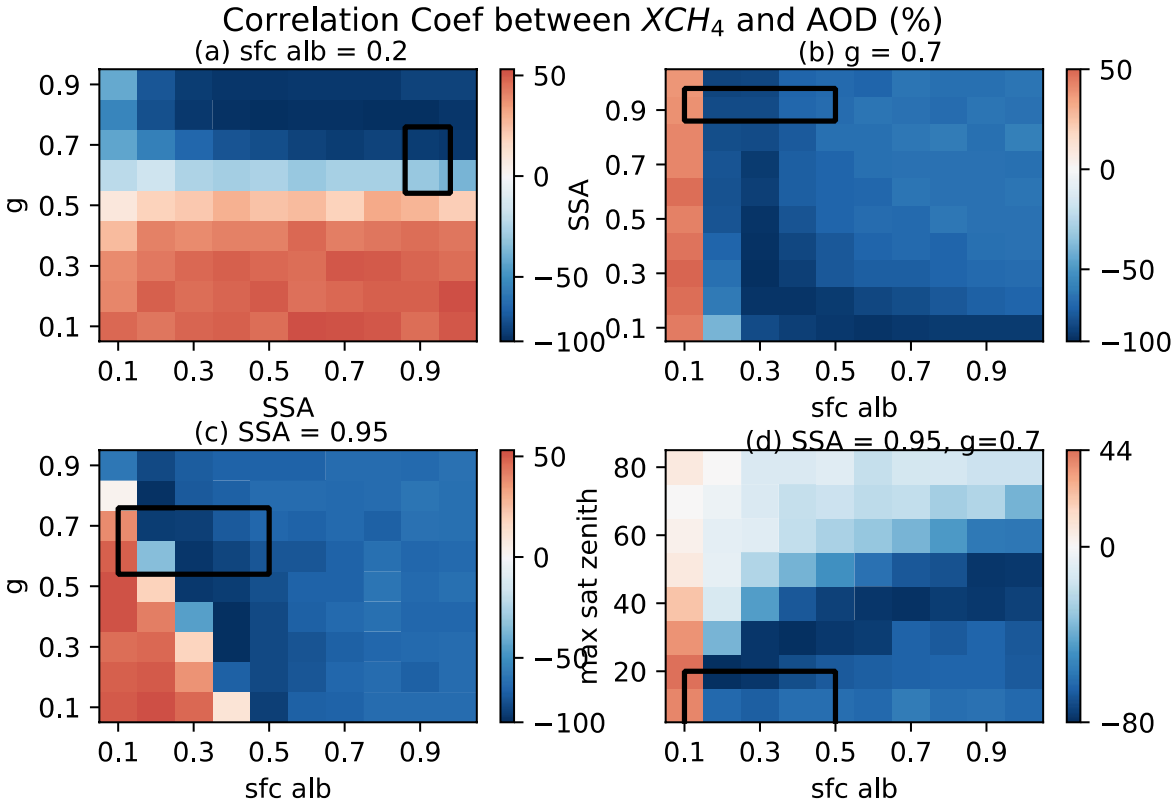

Figure 12. Correlation coefficient (%) between the simultaneously retrieved methane enhancement (ΔX_{CH_4}) and aerosol optical depth (X_{AOD}) when different aerosols are present at different surface albedo values. (a) fix surface albedo as 0.2; (b) fix aerosol g as 0.7; (c) fix aerosol SSA as 0.95. For (a)-(c), the maximum magnitude of the satellite zenith angle is 20°. (d) fix aerosol SSA as 0.95 and g as 0.7.

4 Conclusions

This study investigates the impacts of aerosols on GHGSat methane retrievals in the shortwave near-infrared band by exploiting the dynamic aerosol scattering behaviour during the GHGSat "multi-angle" observation sequence. Specifically, this research assesses how reliably aerosols could be simultaneously retrieved with methane using the multi-angle viewing method under different aerosol optical properties, surface albedo, and satellite zenith angle conditions. Observing system simulation experiments (OSSE) are conducted to simulate GHGSat observations and perform retrievals in the presence of white noise and 1/f errors. These experiments involve a comparative assessment of retrieval accuracy and precision under two conditions: (1) when aerosols are present but not retrieved in the satellite nadir viewing mode and (2) when both methane mixing ratio enhancement (ΔX_{CH_4}) and aerosol optical depth (X_{AOD}) are retrieved simultaneously in the multi-angle viewing mode.

https://doi.org/10.5194/egusphere-2023-2958
Preprint. Discussion started: 23 January 2024

ΔX_{CH_4}-only retrieval experiment indicates the general behaviour that ΔX_{CH_4} is underestimated for low albedo surfaces and overestimated for high albedo surfaces when aerosols are not taken into account. The estimated errors in ΔX_{CH_4} for non-aerosol retrieval become more significant as aerosol single scattering albedo (SSA) increases and asymmetry factor (g) decreases. For nadir viewing simulations where AOD is set at 0.1 and the solar zenith angle at 60°, the mean bias in retrieved ΔX_{CH_4} is most significant when scattering aerosols are neglected over bright surfaces (Fig. 8 & 9). For a surface with a 0.2 albedo, the bias in ΔX_{CH_4} varies from -3.0% to 6.5% for typical aerosol optical properties (SSA ∈ [0.86,0.98] and g ∈ [0.54,0.76]) (Fig. 8a); For satellite zenith angle ranging from 0°-20° and surface albedo varying between 0.1-0.5, the mean bias in ΔX_{CH_4} for ΔX_{CH_4}-only retrieval spans from -5.7%~12.5% (Fig. 11a) assuming an AOD of 0.1, SSA of 0.95 and a g value of 0.7.

Using the multi-angle viewing method for simultaneous ΔX_{CH_4} and X_{AOD} retrieval, we find bias in retrieved ΔX_{CH_4} is significantly reduced at the modest cost of slightly worse ΔX_{CH_4} precision. Through simultaneous retrieval, the mean bias in ΔX_{CH_4} can be reduced to as low as 0.2% for the typical range of aerosol optical properties, surface albedo, and satellite zenith angle (Table 2). The standard deviation (STD) of ΔX_{CH_4} in simultaneous retrieval experiences a slight increase when aerosols have minimum impact on the TOA radiance, indicated by near-zero AOD Jacobian values. Nevertheless, this STD remains within a 2.7% range. Multi-angle viewing methods also perform well in X_{AOD} retrieval, characterized by a near-zero mean bias and a STD of less than 0.05. The performance assessment shows that retrieving aerosols and methane simultaneously using the multi-angle viewing method is a viable approach for operational application to GHGSat.

The correlation coefficient between simultaneously retrieved X_{AOD} and ΔX_{CH_4} switches from positive to negative with the increase of surface albedo and a decrease of aerosol g (Fig. 12a-c). This transition occurs because the dominant influence of aerosols on radiance shifts from the aerosol-only scattering effect to the aerosol-surface multiple scattering effect, which suggests that the ability to differentiate between aerosols and methane is highly dependent on the aerosols and surface conditions.

This study also explored whether the success of the X_{AOD} and ΔX_{CH_4} co-retrieval with multi-angle viewing techniques is largely determined by the range of scattering angles present in the GHGSat observation sequence. After conducting retrievals over a range of satellite zenith angle values (0° to 80°), results suggest that a broader scattering angle range, such as larger satellite zenith angle, has little impact on the improvement of X_{AOD} and ΔX_{CH_4} co-retrieval accuracy and precision. Therefore, the multi-angle viewing method is relatively insensitive to the satellite angle setting for the GHGsat-like instrument when AOD is incorporated in the retrieval.

Finally, future work on the production GHGSat retrieval algorithm and real retrieval test will investigate the feasibility of adding an aerosol retrieval capability for current and future instruments.

https://doi.org/10.5194/egusphere-2023-2958
Preprint. Discussion started: 23 January 2024

Data Availability

The atmospheric model, synthetic data used by the assessment can be obtained from the Mendeley Data (https://mcgill-my.sharepoint.com/:f:/g/personal/qiurun_yu_mail_mcgill_ca/Et1AD0LkLUZCpWD_5i9jE04BteK2aJsgl87LIKaeYjKVkQ?e=XOuWUi).

Author Contribution

QY, DJ, and YH co-designed the OSSEs. QY and YH developed the radiative transfer model and DJ provided the GHGSat instrument model. QY led the writing of the manuscript with contributions from DJ and YH.

Competing Interests

The authors declare that they have no conflict of interest.

Acknowledgments

We acknowledge funding provided by the Mitacs Accelerate program (IT16447) and the Natural Sciences and Engineering Research Council of Canada (Grant RGPIN-2019-04511) that supported this research.

References

Aben, I., Hasekamp, O., and Hartmann, W.: Uncertainties in the space-based measurements of CO2 columns due to scattering in the Earth's atmosphere, Journal of Quantitative Spectroscopy and Radiative Transfer, 104, 450–459, https://doi.org/10.1016/j.jqsrt.2006.09.013, 2007.

Ayash, T., Gong, S. L., Jia, C. Q., Huang, P., Zhao, T. L., and Lavoue, D.: Global modeling of multicomponent aerosol species: Aerosol optical parameters, Journal of Geophysical Research: Atmospheres, 113, https://doi.org/10.1029/2007JD008968, 2008.

Boiyo, R., Kumar, K. R., Zhao, T., and Guo, J.: A 10-Year Record of Aerosol Optical Properties and Radiative Forcing Over Three Environmentally Distinct AERONET Sites in Kenya, East Africa, Journal of Geophysical Research: Atmospheres, 124, 1596–1617, https://doi.org/10.1029/2018JD029461, 2019.

Butz, A., Hasekamp, O. P., Frankenberg, C., and Aben, I.: Retrievals of atmospheric CO_2 from simulated space-borne measurements of backscattered near-infrared sunlight: accounting for aerosol effects, Appl. Opt., 48, 3322, https://doi.org/10.1364/AO.48.003322, 2009.

Butz, A., Galli, A., Hasekamp, O., Landgraf, J., Tol, P., and Aben, I.: TROPOMI aboard Sentinel-5 Precursor: Prospective performance of CH4 retrievals for aerosol and cirrus loaded atmospheres, Remote Sensing of Environment, 120, 267–276, https://doi.org/10.1016/j.rse.2011.05.030, 2012.

https://doi.org/10.5194/egusphere-2023-2958
Preprint. Discussion started: 23 January 2024

Calvello, M., Caggiano, R., Esposito, F., Lettino, A., Sabia, S., Summa, V., and Pavese, G.: IMAA (Integrated Measurements of Aerosol in Agri valley) campaign: Multi-instrumental observations at the largest European oil/gas pre-treatment plant area, Atmospheric Environment, 169, 297–306, https://doi.org/10.1016/j.atmosenv.2017.09.026, 2017.

Chen, X., Yang, D., Cai, Z., Liu, Y., and Spurr, R.: Aerosol Retrieval Sensitivity and Error Analysis for the Cloud and Aerosol Polarimetric Imager on Board TanSat: The Effect of Multi-Angle Measurement, Remote Sensing, 9, 183, https://doi.org/10.3390/rs9020183, 2017.

Clough, S. A., Shephard, M. W., Mlawer, E. J., Delamere, J. S., Iacono, M. J., Cady-Pereira, K., Boukabara, S., and Brown, P. D.: Atmospheric radiative transfer modeling: a summary of the AER codes, Journal of Quantitative Spectroscopy and Radiative Transfer, 91, 233–244, https://doi.org/10.1016/j.jqsrt.2004.05.058, 2005.

Connor, B., Bösch, H., McDuffie, J., Taylor, T., Fu, D., Frankenberg, C., O'Dell, C., Payne, V. H., Gunson, M., Pollock, R., Hobbs, J., Oyafuso, F., and Jiang, Y.: Quantification of uncertainties in OCO-2 measurements of XCO₂:simulations and linear error analysis, Atmos. Meas. Tech., 9, 5227–5238, https://doi.org/10.5194/amt-9-5227-2016, 2016.

Frankenberg, C., Hasekamp, O., O'Dell, C., Sanghavi, S., Butz, A., and Worden, J.: Aerosol information content analysis of multi-angle high spectral resolution measurements and its benefit for high accuracy greenhouse gas retrievals, Atmos. Meas. Tech., 5, 1809–1821, https://doi.org/10.5194/amt-5-1809-2012, 2012.

Houweling, S., Hartmann, W., Aben, I., Schrijver, H., and Skidmore, J.: Evidence of systematic errors in SCIAMACHY-observed CO2 due to aerosols, Atmos. Chem. Phys., 11, 2005.

Huang, J., Arnott, W. P., Barnard, J. C., and Holmes, H. A.: Theoretical Uncertainty Analysis of Satellite Retrieved Aerosol Optical Depth Associated with Surface Albedo and Aerosol Optical Properties, Remote Sensing, 13, 344, https://doi.org/10.3390/rs13030344, 2021.

Huang, Y., Natraj, V., Zeng, Z.-C., Kopparla, P., and Yung, Y. L.: Quantifying the impact of aerosol scattering on the retrieval of methane from airborne remote sensing measurements, Atmos. Meas. Tech., 13, 6755–6769, https://doi.org/10.5194/amt-13-6755-2020, 2020.

Jacob, D. J., Varon, D. J., Cusworth, D. H., Dennison, P. E., Frankenberg, C., Gautam, R., Guanter, L., Kelley, J., McKeever, J., Ott, L. E., Poulter, B., Qu, Z., Thorpe, A. K., Worden, J. R., and Duren, R. M.: Quantifying methane emissions from the global scale down to point sources using satellite observations of atmospheric methane, Gases/Remote Sensing/Troposphere/Chemistry (chemical composition and reactions), https://doi.org/10.5194/acp-2022-246, 2022.

Jervis, D., McKeever, J., Durak, B. O. A., Sloan, J. J., Gains, D., Varon, D. J., Ramier, A., Strupler, M., and Tarrant, E.: The GHGSat-D imaging spectrometer, Atmos. Meas. Tech., 14, 2127–2140, https://doi.org/10.5194/amt-14-2127-2021, 2021.

Lorente, A., Borsdorff, T., Butz, A., Hasekamp, O., Schneider, A., Wu, L., Hase, F., Kivi, R., Wunch, D., and Pollard, D. F.: Methane retrieved from TROPOMI: improvement of the data product and validation of the first 2 years of measurements, Atmospheric Measurement Techniques, 14, 665–684, 2021.

Maasakkers, J. D., Varon, D. J., Elfarsdóttir, A., McKeever, J., Jervis, D., Mahapatra, G., Pandey, S., Lorente, A., Borsdorff, T., Foorthuis, L. R., Schuit, B. J., Tol, P., van Kempen, T. A., van Hees, R., and Aben, I.: Using satellites to uncover large methane emissions from landfills, Science Advances, 8, eabn9683, https://doi.org/10.1126/sciadv.abn9683, 2022.

Parker, R. J., Webb, A., Boesch, H., Somkuti, P., Barrio Guillo, R., Di Noia, A., Kalaitzi, N., Anand, J. S., Bergamaschi, P., Chevallier, F., Palmer, P. I., Feng, L., Deutscher, N. M., Feist, D. G., Griffith, D. W. T., Hase, F., Kivi, R., Morino, I., Notholt,

https://doi.org/10.5194/egusphere-2023-2958
Preprint. Discussion started: 23 January 2024

J., Oh, Y.-S., Ohyama, H., Petri, C., Pollard, D. F., Roehl, C., Sha, M. K., Shiomi, K., Strong, K., Sussmann, R., Té, Y., Velazco, V. A., Warneke, T., Wennberg, P. O., and Wunch, D.: A decade of GOSAT Proxy satellite CH₄ observations, Earth Syst. Sci. Data, 12, 3383–3412, https://doi.org/10.5194/essd-12-3383-2020, 2020.

Sanghavi, S., Nelson, R., Frankenberg, C., and Gunson, M.: Aerosols in OCO-2/GOSAT retrievals of XCO2: An information content and error analysis, Remote Sensing of Environment, 251, 112053, https://doi.org/10.1016/j.rse.2020.112053, 2020.

Stamnes, K., Tsay, S.-C., Wiscombe, W., and Jayaweera, K.: Numerically stable algorithm for discrete-ordinate-method radiative transfer in multiple scattering and emitting layered media, Appl. Opt., AO, 27, 2502–2509, https://doi.org/10.1364/AO.27.002502, 1988.

Thompson, S. N., van Diedenhoven, B., Colarco, P. R., Castellanos, P., Lian, E., and Martins, J. V.: Analysis of Scattering Angle Sampling by Multi-Angle Imaging Polarimeters for Different Orbit Geometries, Frontiers in Remote Sensing, 3, 2022.

Toublanc, D.: Henyey–Greenstein and Mie phase functions in Monte Carlo radiative transfer computations, Appl. Opt., AO, 35, 3270–3274, https://doi.org/10.1364/AO.35.003270, 1996.

Tzanis, C. and Varotsos, C. A.: Tropospheric aerosol forcing of climate: A case study for the greater area of Greece, International Journal of Remote Sensing, 29, 2507–2517, https://doi.org/10.1080/01431160701767575, 2008.

Varon, D. J., McKeever, J., Jervis, D., Maasakkers, J. D., Pandey, S., Houweling, S., Aben, I., Scarpelli, T., and Jacob, D. J.: Satellite Discovery of Anomalously Large Methane Point Sources From Oil/Gas Production, Geophysical Research Letters, 46, 13507–13516, https://doi.org/10.1029/2019GL083798, 2019.

Wang, C., Yang, P., Platnick, S., Heidinger, A. K., Baum, B. A., Greenwald, T., Zhang, Z., and Holz, R. E.: Retrieval of Ice Cloud Properties from AIRS and MODIS Observations Based on a Fast High-Spectral-Resolution Radiative Transfer Model, Journal of Applied Meteorology and Climatology, 52, 710–726, https://doi.org/10.1175/JAMC-D-12-020.1, 2013.

Yu, Q. and Huang, Y.: Distributions and Trends of the Aerosol Direct Radiative Effect in the 21st Century: Aerosol and Environmental Contributions, JGR Atmospheres, 128, https://doi.org/10.1029/2022JD037716, 2023.